IOP Conference Series: Materials Science and Engineering

First principles evaluation on photocatalytic suitability of 2*H* structured and [0001] oriented WS_2 nanosheets and nanotubes

IOP Conf. Series: Materials Science and Engineering **503** (2019) 012002 doi:10.1088/1757-899X/503/1/012002

First principles evaluation on photocatalytic suitability of 2*H* structured and [0001] oriented WS_2 nanosheets and nanotubes

Y F Zhukovskii[1], S Piskunov[1] and R A Evarestov[2]

[1]Institute of Solid State Physics, University of Latvia, 8 Kengaraga Street, LV-1083 Riga, Latvia
[2]St. Petersburg State University, 7/9 Universitetskaya nab., 199034 St. Petersburg, Russia

e-mail: sergejs.piskunovs@cfi.lu.lv

Abstract. Pristine WS_2 multilayer nanosheets (NSs), which thickness h_{NS} varies from 1 to 12 monolayers (MLs), as well as single- and multi-walled nanotubes (SW and MW NTs) of different chirality, which diameter d_{NT} exceeds 1.9 nm, display photocatalytic suitability to split H_2O molecules. Obviously, such a phenomenon can occur since the band gap of these nanostructures corresponds to the energy range of visible light between the red and violet edges of spectrum (1.55 eV < $\Delta\varepsilon_{gap}$ < 2.65 eV). For all the studied WS_2 NSs and NTs, the levels of the top of the valence band and the bottom of the conduction band must be properly aligned relatively to H_2O oxidation and reduction potentials separated by 1.23 eV: $\varepsilon_{VB} < \varepsilon_{O_2/H_2O} < \varepsilon_{H^+/H_2} < \varepsilon_{CB}$. The values of $\Delta\varepsilon_{gap}$ decrease with growth of h_{NS} and increase with enlargement of d_{NT}. 1 ML nanosheet can be considered as a limit of infinite SW NT thickness growth ($d_{NT}\to\infty$), which band gap increases up to ~2.65 eV. First principles calculations have been performed using the hybrid DFT-HF method (HSE06 Hamiltonian) adapted for 2*H* WS_2 bulk. The highest solar energy conversion efficiency (15-18%) expected at $\Delta\varepsilon_{gap}$ = 2.0-2.2 eV (yellow-green range) has been found for 2 ML thick (stoichiometric) WS_2 (0001) NS as well as WS_2 NTs with diameters 2.7-3.2 nm (irrespectively on morphology and chirality indices *n* of nanotubes). Moreover, unlike discrete variation of h_{NS} magnitudes, tuning of d_{NT} values provides much higher energy resolution.

1. Introduction

Photocatalytic water splitting under influence of solar light in vicinity of semiconducting electrode immersed in aqueous medium is a clean and renewable source for the production of hydrogen fuel [1], which plays essential role in contemporary energetics. A number of semiconductors of various chemical nature, dimensionality and morphology were studied previously as potential candidates for photocatalytic electrodes, including transition metal dichalcogenides (TMDC) attracting enhanced attention during last 10-15 years due to the progress in their fabrication and application [2]. The optimum band gap of semiconducting electrode for dissociation of H_2O molecules caused by the influence of visible light lies in the range of 2.0–2.2 eV [3]. Absorption of photons results in migration of excited electrons over the bottom of conduction band (CB), which simultaneously creates holes under the top of valence band. Since centers of dissociation located on the catalyst surface are important for the water splitting in order to prevent recombination between electrons and holes [4], reproducible fabrication of nanostructures is one of ways how to ensure the direct exit of recombination centers to the surface, thus noticeably enhancing photocatalytic efficiency. First of all 2D nanothin films, 1D nanotubes and nanoribbons as well as 0D fullerene-like nanocages and nanoclusters can be applied for photocatalytic splitting of water. In the current study, we analyze periodic nanosystems only.

Morphology of TMDC bulk materials can be presented in the form of 1*T*, 2*H* and 3*R* phases corresponding to trigonal, hexagonal as well as rhombohedral crystalline lattices described by D_{3d}, D_{3h} and C_{3v}^5 point groups, respectively [5]. These types of crystals establish the class of two-periodic layered structures characterized by strong chemical (mainly covalent) bonds within the single monolayers (MLs) and weak coupling between the neighboring MLs. Of particular interest is their high catalytic activity

towards the hydrogen evolution reaction [6], which could support efficient and low-cost production of hydrogen without reliance on expensive Pt-based catalysts. The most widespread two-periodic transition metal dichalcogenides applied for photocatalytic splitting of water and other molecules were found to be MoS_2 and WS_2 disulfides [7], which prefer to be stacked in $2H\,c$ bulk phase and can be "restacked" from separate graphene-like monolayers when using the corresponding experimental methods [8].

When applying the layered TMDC materials engineering, various experimental techniques (*e.g.*, atomic force microscopy and optical contrast) provide precise control of perfectness and thickness of nanothin films deposited on supporting substrates [9]. Atomically thin WS_2 nanosheets were prepared applying sulfurization of the ultrathin WO_3 films [10] by adjusting the number of plasma enhanced atomic layer deposition during the process cycles. The high uniformity of mono-, bi-, and tetra-layered WS_2 films synthesized upon α-Al_2O_3 and SiO_2/Si substrates was achieved when using the low-pressure chemical vapor deposition (CVD) method [11, 12] which is predominantly applied until now. Mechanically exfoliated WS_2 flakes consisting of a few monolayers covered the transparent quartz or SiO_2/Si substrates with incorporated iodine (providing abundant active edges for photocatalytic reactions) were carefully studied using CVD method too [13]. Nanothin films consisting of a few WS_2 monolayers were also experimentally observed to grow upon [0001]-oriented ZnO nanowires [14], formation of which was confirmed by using the methods of transmission electron microscopy, Raman scattering and optical spectroscopy. Photoluminescence of WS_2 nanosheets, as reported recently [15], weakens with increasing number of monolayers due to a transition from the direct band gap in a monolayer to the indirect gap in multilayers.

To determine the band structure of WS_2 single crystal and monolayer, both augmented spherical wave calculations based on density functional theory (DFT) and angle-resolved photoelectron spectroscopy using synchrotron radiation source were applied [16]. Comprehensive DFT plane wave study of the electronic structure and photocatalytic properties for a number of TMDC single MX_2 monolayers was performed recently [17] using many-body G_0W_0 Green function approach and either GGA PBE [18] or hybrid HSE06 functionals [19]. In order to estimate the proper alignment of the top of valence band ε_{VB} and the bottom of conduction band ε_{CB} with the oxidation and reduction potentials (ε_{O_2/H_2O} and ε_{H^+/H_2}, respectively) as a criterion of photocatalytic suitability, the quasiparticle band gap was constructed relatively to its center following the method proposed by Toroker *et al* [20].

For the first time, R. Tenne *et al.* synthesized WS_2 nanotubes (NTs) in 1992 [21] following the later intensive experimental studies on them. For example, a successful attempt to synthesize Nb-doped WS_2 NTs was undertaken [22], which inhibits the formation of defective nanotubes unlike routine synthesis of pristine nanotubes. Controlled Re-doping of WS_2 nanotubes and fullerene-shaped structures resulted in a drop of the electrical resistivity, leading to a more efficient electron transport through the corresponding nanotubes [23]. Combination of metallic Co nanoparticles and semiconducting WS_2 NTs results in essential enhancement of the photoactivity of hybrid nanostructures [24]. Therefore, efficient light absorption by nanotubes can occur and subsequent charge separation between the semiconducting WS_2 nanotube and the metallic nanocluster takes place under visible light illumination.

However, theoretical characterization of WS_2 NTs is still in its infancy [25, 26]. The latter took into account approaches based on the line symmetry group formalism, using either valence force-fields combined with semi-empirical density functional tight binding theory (DFTB) [25] or an *ab initio* hybrid DFT-HF formalism using the HSE06 functional in which the DFT Hamiltonian is extended by inclusion of Hartree-Fock (HF) exchange and correlation [26]. Recent *ab initio* calculations have focused on comparison between the electronic structures in WS_2 bulk as well as its layered and nanotubular forms [27]. In those publications and additionally in Ref. [28] both vibrational and electronic properties of WS_2 NTs were calculated and analyzed, however, not their possible photocatalytic applications.

To fill the gap existing in comprehensive investigations of WS_2 monoperiodic structures, especially their photocatalytic suitability for water splitting, we have evaluated recently various WS_2 nanosheets [9] and nanotubes [29] performing for this aim large-scale *ab initio* calculations on their electronic structure. In this study, we compare the corresponding results to estimate which efficiency is higher.

2. Theoretical background

2.1. Hybrid DFT&HF-LCAO method

Large scale *ab initio* calculations on [0001]-oriented WS_2 nanosheets and nanotubes with varied thickness h_{NS} and diameter d_{NT}, respectively, have been performed using the hybrid density functional theory (DFT)/Hartree-Fock (HF) calculations using the *CRYSTAL14* computer code [30]. It utilizes localized Gaussian type functions (GTFs) in the form of atom-centered basis sets (BSs) for expansion of periodic crystalline orbitals as linear combinations of atomic orbitals (LCAO). We have used the HSE06 hybrid functional [19], which proved to be the most adequate for reproducing the experimental value of band gap for tungsten disulfide bulk (1.58 eV *vs.* 1.4 eV obtained in our fully relaxed calculations [9] and experimental measurements [31], respectively). Balanced summation in both direct and reciprocal WS_2 nanosheets and nanotubes requires choice of the reciprocal space integration by sampling the Brillouin zone (BZ) with 18×18×1 and 18×1×1 Monkhorst−Pack meshes [32], respectively, which result in total of 37 and 10 *k*-points evenly distributed over the corresponding BZs. For the fixed crystalline geometry, calculations converge when the total energy differs by less than 10^{-9} a. u. in two successive cycles of the self-consistent field (SCF) procedure [30]. Full geometry optimization has been performed for all considered in this study WS_2 bulk, slab and tubular models.

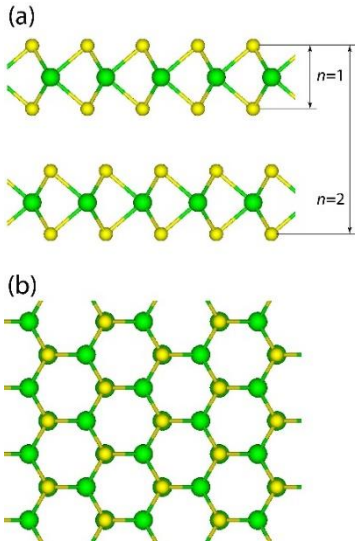

Figure 1. Models of single- and double-layered WS_2 (0001) nanosheets described by hexagonal symmetry of 2*H c* phase (aside (a) and atop (b) views). W and S atoms are marked with large green (dark) balls and small yellow (light) balls, respectively.

2.2. Models of WS_2 nanosheets and nanotubes

The primitive unit cell of hexagonal 2*H c* phase mentioned above as the most stable for WS_2 bulk consists of two atomic inversely arranged layers containing three atomic planes each [14]. Inner planes of each WS_2 layer contain only tungsten atoms while in its turn outer planes contain sulfur atoms. Due to weak interaction forces acting between monolayers, as considered above, the inter-layer distance, which corresponds to a half of the lattice constant *c* for bulk tungsten disulphide) is essentially larger (6.16 Å) as compared to the constant *a* (3.15 Å) [14]. In order to check the photocatalytic suitability of graphene-type WS_2 (0001) nanosheets with varied thicknesses h_{NS}, we have constructed stacks of 1-12 MLs (corresponding to 0.31-5.91 nm thickness) and, additionally, models containing up to 20, 30, and 40 MLs. Models of tungsten disulfide nanothin films consisting of single- and double-layered are shown in Figure 1. Nanosheets containing odd (1, 3, 5, . . ., 2*n*+1 MLs) and even (2, 4, 6, . . ., 2*n* MLs) numbers of WS_2 monolayers, where $n = 0$, 1, 2, . . ., possess two different layer symmetry groups $P\bar{6}m2$ and $P\bar{3}m1$, respectively.

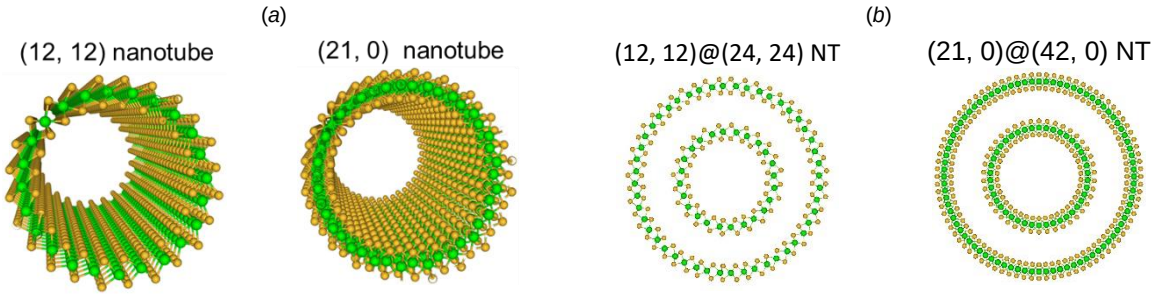

Figure 2. Models of SW (*a*, axonometric images) and DW (*b*, cross-sections perpendicular to NT axes) [0001]-oriented WS_2 nanotubes possessing armchair (*n*, *n*) and zigzag-type (*n*, 0) chiralities. W and S atoms are marked with large dark balls and small light balls, respectively.

Construction of [0001] oriented WS_2 NTs described by folding the corresponding nanolayer results in formation of the cylindrical nanotubes by rolling up the graphene-structured nanosheets using the formalism of line groups [25, 26]. For this purpose the nomenclature of single-walled (*m*, *n*) carbon nanotubes can be expressed *via* the so-called chirality indices *m* and *n* as described earlier [33]. To clarify dependence of photocatalytic suitability on NT morphology, we have performed *ab initio* calculations on WS_2 NTs with both achiral single-walled armchair (*n*, *n*) and zigzag-type (*n*, 0) structure and diameters d_{NT} > 1.0 nm (Figure 2a) as well as double-walled (*m*, *m*)@(*n*, *n*) and (*m*, *0*)@(*n*, 0) nanotubes, internal diameters of which exceed 1.0 nm (Figure 2b).

The achiral armchair (*n*, *n*) and zigzag (*n*, 0) single-walled tungsten disulphide nanotubes with hexagonal morphology belong to 4 and 8 line-group families with $L(2n)_n/m$ and $L(2n)_n$ *mc* symmetry, accordingly [26]. Both types of WS_2 NTs with achiral morphology possess the helical axes of order 2*n*.

3. Results of calculations, their analysis and comparison

3.1. Suitability of periodic pristine WS_2 nanostructures for photocatalytic applications

Several special conditions are required for a material to be photocatalytically active for water splitting. First, the band gap of the catalyst must correspond to the visible light range between 1.5-2.7 eV. For the solar intensity distribution, the maximum efficiency is achievable for a band gap between 2.0 and 2.2 eV. The energy conservation condition requires that both the oxidation and the reduction potentials of the H_2O molecule in solution defined thermodynamically (ε_{O_2/H_2O} = -5.67 eV and ε_{H^+/H_2} = - 4.44 eV) [1] must be positioned inside the band gap of the photocatalytic electrode. Thus, the following inequalities have to be hold:

$$\varepsilon_{VB} < \varepsilon_{O_2/H_2O} < \varepsilon_{H^+/H_2} < \varepsilon_{CB}. \quad (1)$$

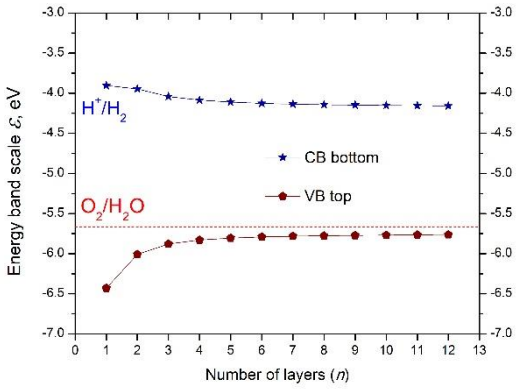

Figure 3. Dependence of WS_2 (0001) band gap parameters on nanolayer thickness with alignment of ε_{CB} and ε_{VB} edges relative to the redox potentials.

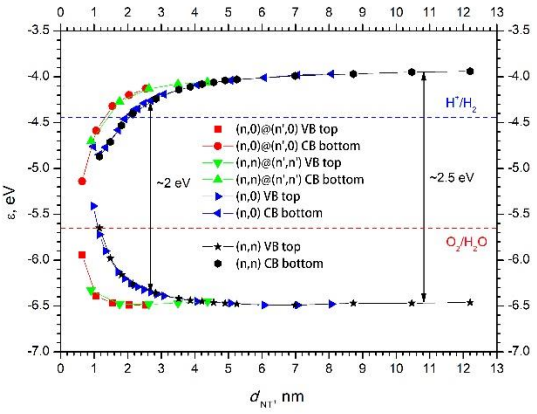

Figure 4. Dependence of band gap parameters for SW and DW WS_2 NTs on the values of d_{NW} (inner for DW) with alignment of ε_{CB} and ε_{VB} edges relative to ε_{O_2/H_2O} and ε_{H^+/H_2} levels.

Figures 3 and 4 present results of our calculations on the band edge parameters of twelve WS_2 nanosheets and approximately forty different nanotubes, respectively, including the positions of ε_{O_2/H_2O} and ε_{H^+/H_2} at the energy scale. One can see that levels of ε_{VB} for all NSs and NTs are always below the ε_{O_2/H_2O} level; thus, the left part of Eq. (1) is satisfied for all nanotubes. In contrary, if for all nanosheets the right part of Eq. (1) is always satisfied, then for thin NTs (d_{NT} < 1.9 nm), the level of ε_{CB} is located below the ε_{O_2/H_2O}, which prevents the catalytic decomposition of H_2O molecules. However, further increase of d_{NT} leads to a rapid shift of the ε_{CB} level upward, thus, Eq. (1) is valid for all nanotubes, diameter of which exceeds 1.9 nm, irrespective of chirality. We note that the increase of the band gap of nanosheets with

reduced thickness can be attributed to the quantum confinement effect, while in nanotubes the strain effect is predominant and therefore the bandgap shrinks with reducing nanotube's diameter.

3.2 Comparison of band structure for double- and monoperiodic pristine WS_2 nanostructures

We have performed recently detailed analysis of DOSs for WS_2 nanosheets [9] and nanotubes [29]. In this study, we analyze and compare the band structure of tungsten disulphide nanosheets and two achiral nanotubes, respectively. In Figure 5, we compare the band structures of WS_2 (0001) monolayer and bilayer using Γ(0, 0, 0) – M(1/2, 0, 0) – K(1/3, 1/3, 1/3) – Γ(0, 0, 0) paths for both in the Brillouin Zone. In the case of 1 ML, the optical direct band gap is located at K-point. For bilayers and more thick nanosheets, we observe indirect gaps only. When the number of monolayers increases, the fundamental band gap decreases and tends to bulk value.

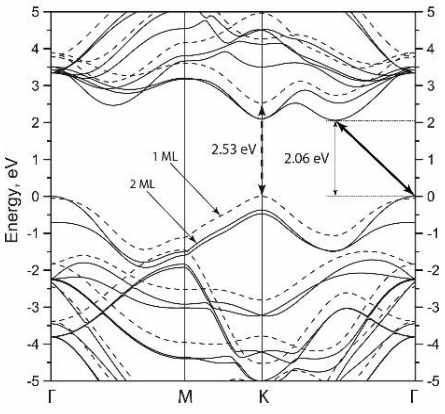

Figure 5. Band structure for WS_2 NSs consisting of 1 ML (dashed lines) and 2 ML (solid lines).

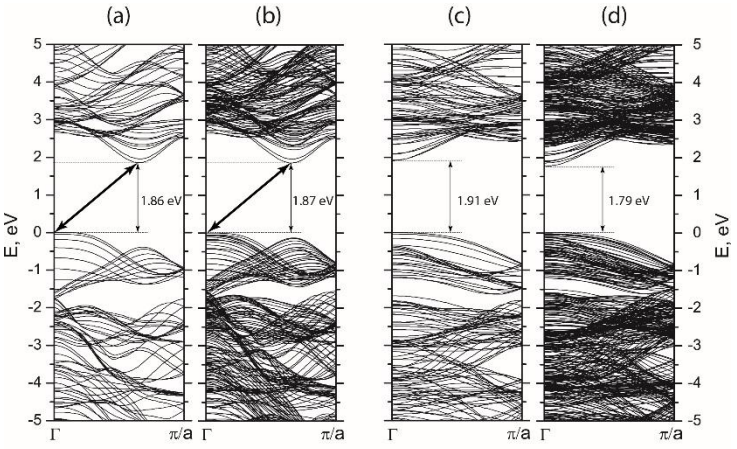

Figure 6. Band structure for WS_2 NTs possessing armchair and zigzag-type chiralities: (a) SW (12,12) WS_2 NT, (b) DW (12,12)@(24,24) WS_2 NT, (c) SW (21,0) WS_2 NT, and (d) DW (21,0) @(42,0) WS_2 NT.

In the case of both achiral SW and DW WS_2 NTs (Figure 6), the indirect band gaps characterize armchair (*ac*) chirality (a, b), while for zigzag-type (*zz*) nanotubes, our calculations yield direct Γ– Γ band gap, irrespectively to the number of NT walls (c, d). These results contradict to conclusion drawn for band structures of single- and double-layered WS_2 (0001) nanosheet (Figure 5) characterized by direct and indirect transitions from the bottom of the CB to the top of the VB, respectively.

4. Conclusions

We have simulated the electronic structure of pristine WS_2 multilayer nanosheets with varied thickness as well as single- and double-walled WS_2 nanotubes of different chirality with varied diameter. 2D-peiodic nanostructures are found suitable for photocatalytic applications since their band gaps correspond to the whole range of visible light between the red and violet edges (1.5 eV < $\Delta\varepsilon_{gap}$ < 2.7 eV) while the top of valence band and the bottom of conduction band are properly aligned relative to the oxidation and reduction potentials, *i.e.*: $\varepsilon_{VB} < \varepsilon_{O_2/H_2O} < \varepsilon_{H^+/H_2} < \varepsilon_{CB}$.

The only limitation for photocatalytic suitability of WS_2 NTs is determined by $d_{NT} > 1.9$ nm (for DW NTs, this condition concerns the internal wall). On the other hand, tuning of d_{NT} provides much higher energy resolution than in the case of nanosheets. Moreover, energies of $\Delta\varepsilon_{gap}$ edges depend only on diameter d_{NT} (increasing monotonously with increasing diameter) and do not depend on chirality indices *n*. Principal difference between both types of WS_2 nanostructures is that the value of $\Delta\varepsilon_{gap}$ for nanotubes grows with increasing d_{NT}, while that of nanosheets decreases with enlargement of h_{NS}. Furthermore, the bandgap of DW NT is smaller than the corresponding$\Delta\varepsilon_{gap}$ values for each of its constituents.

The highest conversion efficiency of single-walled nanotubes is achieved between the yellow-green ranges of visible spectrum ($2.0 < \Delta\varepsilon_{gap} < 2.2$ eV), which corresponds to diameter variation 2.7 nm < d_{NT} < 3.2 nm, irrespectively on chirality. For WS_2 (0001) nanosheets, the highest photocatalytic efficiency is achieved for 2 ML thickness due to discreteness of h_{NS} values, thus giving a preference to nanotubes.

Acknowledgements
This study was supported by the EC ERA.Net RUS Plus Project No. 237 WATERSPLIT. R.E. acknowledges the financial support provided by the Russian Foundation for Basic Research (grant N 17-03-00130a) and High Performance Computer Center of St. Petersburg University for the assistance. The authors are indebted to D. Bocharov, O. Lisovski and E. Spohr for stimulating discussions.

References

[1] Chen X, Shen S, Guo L and Mao S S 2010 *Chem. Rev.* **110** 6503
[2] Dong R and Kuljanishvili I 2017 *J. Vacuum Sci. Technol. B* **35** 030803
[3] Navarro R M, Alvarez-Galvan M C, Villoria de la Mano J A, Al-Zahrani S M and Fierro J L G 2010 *Energy Environ. Sci.* **3** 1865
[4] Kudo A and Miseki Y 2009 *Chem. Soc. Rev.* **38** 253
[5] Toh R J, Sofer Z, Luxa J, Sedmidubsky D and Pumera M 2017 *Chem. Commun.* **53** 3054
[6] Benck J D, Hellsternn T R, Kibsgaard J, Chakthranont P and Jaramillo T F 2014 *ACS Catal.* **4** 3957
[7] Chen T E, Chang Y H, Hsu C L, Wei K H, Chiang C Y and Li L J 2013 *Int. J Hydrogen Energy* **38** 12302
[8] Petkov V, Billinge S J L, Heising J and Kanatzidis M G 2000 *J. Am. Chem. Soc.* **122** 11571
[9] Bocharov D, Piskunov S, Zhukovskii Y F and Evarestov R A 2018 *phys. status solidi rrl* **12** 1800253
[10] Zeng W. Feng L-P, Su J, Pan H-xi and Liu Z-T 2018 *J. Alloys&Compd.* **745** 834
[11] Zhang Y, Zhang Y, Ji Q, Ju J, Yuan H, Shi J, Gao T, Ma D, Liu M, Chen Y, Song X, Hwang H Y, Cui Y and Liu Z 2013 *ACS Nano* **7** 8963
[12] Park J, Lee W, Choi T, Hwang S-H, Myoung J M, Jung J-H, Kim S-H and Kim H 2015 *Nanoscale* **7** 1308
[13] Zhao W, Ghorannevis Z, Chu L, Toh M, Kloc C, Tan P-H and Eda G 2013 *ACS Nan*o **7** 791
[14] Polyakov B, Kuzmin A, Smits K, Zideluns J, Butanovs E, Butikova J, Vlassov S, Piskunov S and Zhukovskii Y F 2016 *J. Phys. Chem. C* **120** 2145
[15] Gutiérrez H R, Peres-López N, Elias A L, Berkdemir A, Wang B, Lv R, López-Urias F, Crespi V, Terrones H and Terrones M 2013 *Nano Lett.* **13** 3447
[16] Klein A, Tiefenbacher S, Eyert V, Pettenkofer C and Jaegermann W 2001 *Phys. Rev. B* **64** 205416
[17] Zhuang H L and Hennig R G 2013 *J. Phys. Chem. C* **117** 20440
[18] Perdew J P, Burke K and Ernzerhof M 1996 *Phys. Rev. Lett.* **77**, 3865
[19] Heyd J, Scuseria G E, and Ernzerhof M 2003 *J. Chem. Phys.* **118** 8207
[20] Toroker M C, Kanan D K, Alidoust N, Isseroff L Y, Liao P and Carter E A 2011 *Phys. Chem. Chem. Phys.* **13** 16644
[21] Tenne R, Margulis L, Genut M and Hodes G 1992 *Nature* **360** 444
[22] Zhu Y Q, Hsu W K, Firth S, Terrones, M, Grobert N, Clark R J H, Kroto H W, Walton D R M 2001 *Chem. Phys. Lett.* **342** 15
[23] Yadgarov L, Rosentsveig R, Leitus G, Albu-Yaron A, Moshkovich A, Perfilyev V, Vasic R, Frenkel A I, Enyashin A N, Seifert G, Rapoport and Tenne R 2012 *Angew. Chemie Intl. Ed. Engl.* **51** 1148
[24] Tsverin Y, Livneh T, Rosentsveig R, Zak A, Pinkas I and Tenne R. 2013 *Nanomater. Energy* **2** 25
[25] Damnjanović M, Vuković T and Milošević I 2017 *Isr. J. Chem.* **57** 450
[26] Evarestov R A, Bandura A V, Porsev V V and Kovalenko A V 2017 *J. Comput. Chem.* **38** 2581
[27] Zibouche N, Kuc A and Heine T 2012 *Eur. Phys. J. B* **85** 1

[28] O'Neal K R, Cherian J G, Zak A, Tenne R, Liu Z and Musfeldt J L 2016 *Nano Lett.* **16** 993
[29] Piskunov S, Lisovski O, Zhukovskii Y F, Dyachkov P N, Evarestov R A, Kenmoe S and Spohr E 2018 *ACS Omega* **4** 1434
[30] Dovesi R, Saunders V R, Roetti C, Orlando R, Zicovich-Wilson C M, Pascale F, Civalleri B, Doll K, Harrison N M, Bush I J, D'Arco Ph, Llunell M, Causá M and Noël Y 2014 *CRYSTAL14 User's Manual*, University of Torino
[31] Braga D, Gutiérrez Lezama I, Berger H and Morpurgo A F 2012 *Nano Lett.* **12** 5218
[32] Monkhorst H J and Pack J D 1976 *Phys. Rev. B* **13** 5188
[33] Saito R, Dresselhaus M S and Dresselhaus G 1998 *Physical Properties of Carbon Nanotubes*.(Imperial College Press, World Scientific Publishing Co. Pte. Ltd., Singapore)